

Respiratory disease in rhesus macaques inoculated with SARS-CoV-2

<https://doi.org/10.1038/s41586-020-2324-7>

Received: 22 March 2020

Accepted: 1 May 2020

Published online: 12 May 2020

 Check for updates

Vincent J. Munster¹, Friederike Feldmann², Brandi N. Williamson¹, Neeltje van Doremale¹, Lizzette Pérez-Pérez¹, Jonathan Schulz¹, Kimberly Meade-White¹, Atsushi Okumura¹, Julie Callison¹, Beniah Brumbaugh³, Victoria A. Avanzato¹, Rebecca Rosenke², Patrick W. Hanley², Greg Saturday², Dana Scott², Elizabeth R. Fischer³ & Emmie de Wit¹✉

An outbreak of coronavirus disease 2019 (COVID-19), which is caused by a novel coronavirus (named SARS-CoV-2) and has a case fatality rate of approximately 2%, started in Wuhan (China) in December 2019^{1,2}. Following an unprecedented global spread³, the World Health Organization declared COVID-19 a pandemic on 11 March 2020. Although data on COVID-19 in humans are emerging at a steady pace, some aspects of the pathogenesis of SARS-CoV-2 can be studied in detail only in animal models, in which repeated sampling and tissue collection is possible. Here we show that SARS-CoV-2 causes a respiratory disease in rhesus macaques that lasts between 8 and 16 days. Pulmonary infiltrates, which are a hallmark of COVID-19 in humans, were visible in lung radiographs. We detected high viral loads in swabs from the nose and throat of all of the macaques, as well as in bronchoalveolar lavages; in one macaque, we observed prolonged rectal shedding. Together, the rhesus macaque recapitulates the moderate disease that has been observed in the majority of human cases of COVID-19. The establishment of the rhesus macaque as a model of COVID-19 will increase our understanding of the pathogenesis of this disease, and aid in the development and testing of medical countermeasures.

SARS-CoV-2 infection in humans can be asymptomatic or result in mild-to-fatal COVID-19^{4–6}. Patients with COVID-19 who develop pneumonia have presented mainly with fever, fatigue, dyspnoea and a cough^{7–9}. Rapidly progressing pneumonia—with bilateral opacities on X-rays or patchy shadows and ground-glass opacities by computed tomography scan—has been observed in patients with COVID-19^{2,6,10}. Older patients with comorbidities are at the highest risk of an adverse outcome of COVID-19^{5,7}. SARS-CoV-2 has been detected in samples from the upper and lower respiratory tracts of patients with COVID-19, in faeces and in blood, but not in urine^{5,11–13}.

Non-human-primate models that recapitulate aspects of human disease are essential for our understanding of the pathogenic processes involved in severe respiratory disease and for the development of medical countermeasures such as vaccines and antiviral agents.

Clinical respiratory disease

We inoculated eight adult rhesus macaques with the SARS-CoV-2 isolate nCoV-WA1-2020¹⁴. On day 1 post-inoculation (dpi), all macaques showed changes in their respiratory pattern and piloerection, as reflected in their clinical scores (Fig. 1a). Other signs of disease we observed included reduced appetite, a hunched posture, pale appearance and dehydration (Extended Data Table 1). Coughing was occasionally heard in the room where macaques were housed, but could not be pinpointed

to individual macaques. Signs of disease persisted for more than a week, with all macaques being completely recovered between 9 and 17 dpi (Fig. 1a, Extended Data Table 1). We observed weight loss in all macaques (Fig. 1b); body temperatures spiked at 1 dpi but returned to normal levels thereafter (Fig. 1c). Under anaesthesia, the macaques did not show increased respiration; however, all macaques showed irregular respiration patterns (Fig. 1d). Radiographs showed pulmonary infiltrates in all macaques, starting at 1 dpi with mild pulmonary infiltration primarily in the lower lobes of the lung. By 3 dpi, we noted progression of mild pulmonary infiltration into other lung lobes, although these infiltrates were still primarily located in the caudal lung lobes (Fig. 1e). In one macaque, pulmonary infiltrates were observed from 1 to 12 dpi (Extended Data Fig. 1).

Haematological analysis of blood collected during clinical examinations showed a stress leukogram¹⁵ by 1 dpi in the majority of macaques (Extended Data Fig. 2). Lymphocytes and monocytes began to return baseline levels after 1 dpi. Neutrophils had begun to decrease in all macaques by 3 dpi, and continued to decline through to 5 dpi; in 2 of 4 macaques, this led to neutropenia. We observed decreased haemoglobin, red blood cell counts and haemoglobin in all macaques at 1 dpi (Extended Data Fig. 2). In addition, reticulocyte percentages and counts had also decreased by this time point. At 5 dpi, 2 of 4 macaques had a normocytic, normochromic nonregenerative anaemia (consistent with the anaemia of a critical illness); these macaques had not returned

¹Laboratory of Virology, National Institute of Allergy and Infectious Diseases, National Institutes of Health, Hamilton, MT, USA. ²Rocky Mountain Veterinary Branch, National Institute of Allergy and Infectious Diseases, National Institutes of Health, Hamilton, MT, USA. ³Research Technologies Branch, National Institute of Allergy and Infectious Diseases, National Institutes of Health, Hamilton, MT, USA. ✉e-mail: emmie.dewit@nih.gov

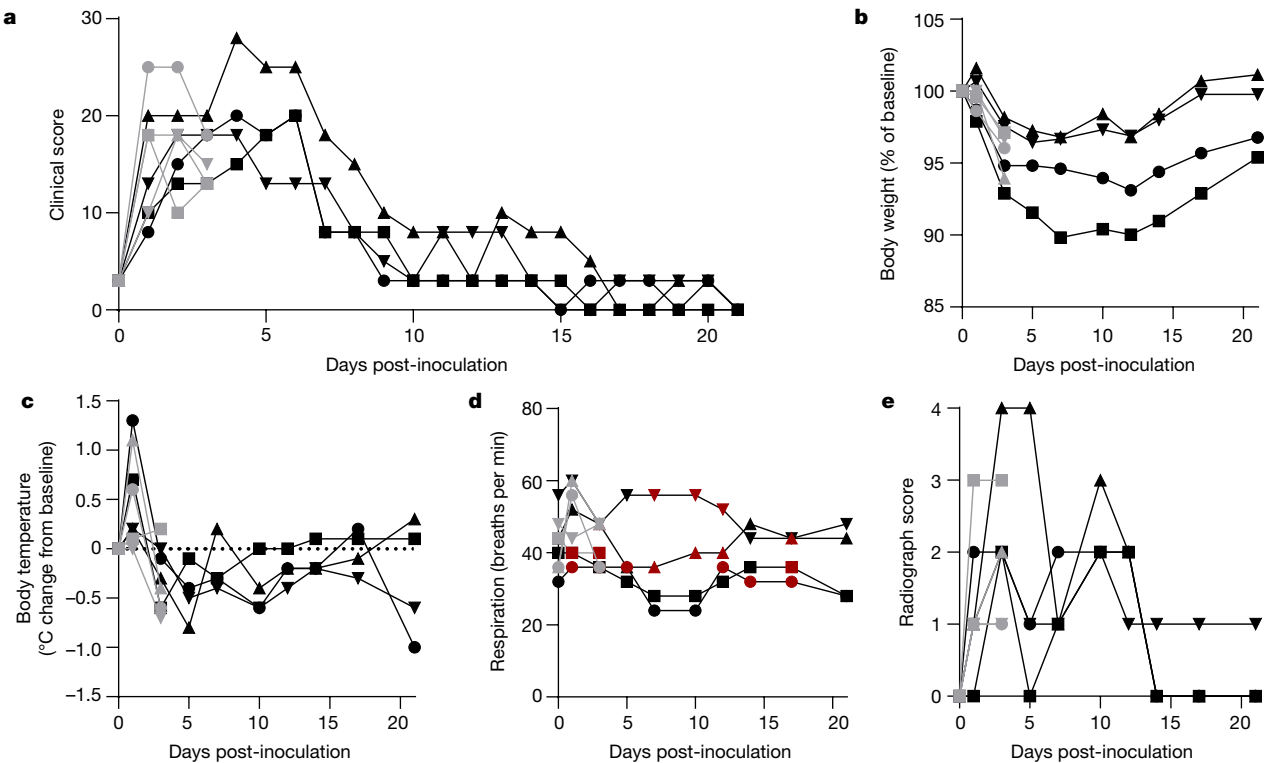


Fig. 1 | Rhesus macaques infected with SARS-CoV-2 develop respiratory disease. **a**, After inoculation with SARS-CoV-2, macaques were observed for signs of disease, and scored according to a pre-established clinical scoring sheet. **b, c**, Body weight (**b**) and body temperature (**c**) were measured in clinical examinations. **d**, Respiration rate was measured, and breathing pattern was recorded; irregular respiration patterns are indicated in red. **e**, Ventrodorsal and lateral radiographs were taken on days on which clinical examination were performed, and were scored for the presence of pulmonary infiltrates: 0,

normal; 1, mild interstitial pulmonary infiltrates; 2, moderate pulmonary infiltrates (sometimes with partial effacement of the cardiac border and small areas of pulmonary consolidation); 3, severe interstitial infiltrates, large areas of pulmonary consolidation, alveolar patterns and air bronchograms. Individual lobes were scored, and scores per macaque per day were totalled. Grey, macaques that were euthanized at 3 dpi ($n=4$); black, macaques that were euthanized at 21 dpi ($n=4$). The symbols used to denote specific individual macaques are identical throughout the Article.

to their original baseline measurements by 21 dpi. Blood chemistry analysis revealed no values outside of the normal range (Supplementary Table 2).

We analysed serum for changes in cytokine and chemokine levels at different time points after inoculation. We observed statistically significant changes only at 1 dpi (when there were increases in IL-1RA, IL-6, IL-10, IL-15, MCP-1 and MIP-1 β) and at 3 dpi, when a small—but statistically significant—decrease in TGF α occurred (Extended Data Fig. 3). Although the levels of some of these cytokines changed at later time points after inoculation, these changes were not statistically significant (Extended Data Fig. 3).

High viral loads in respiratory samples

Virus shedding was highest from the nose (Fig. 2a); virus could be isolated from swabs collected at 1 and 3 dpi, but not thereafter. Viral loads were high in throat swabs immediately after inoculation, but were less consistent than nose swabs thereafter; in one macaque, throat swabs were positive at 1 dpi and at 10 dpi—but not in between (Fig. 2a). One macaque showed prolonged shedding of viral RNA in rectal swabs; infectious virus could not be isolated from these swabs (Fig. 2a) and disease of the intestinal tract (for example, diarrhoea) was not observed. Urogenital swabs remained negative in all macaques throughout the study. For the 4 macaques in the group that was euthanized at 21 dpi, we performed bronchoalveolar lavages at 1, 3 and 5 dpi. We detected high viral loads in fluid from the bronchoalveolar lavage in all macaques at all three time points; infectious virus could be isolated only from bronchoalveolar fluid collected at 1 and 3 dpi (Fig. 2b). No viral RNA was detected in the blood (Fig. 2c) or urine (Fig. 2d).

Interstitial pneumonia

Two groups of 4 macaques were euthanized (one at 3 dpi and the other at 21 dpi), and necropsies were performed. At 3 dpi, varying degrees of lung lesions at the gross pathological scale were observed in all macaques (Fig. 3a, c). At 21 dpi, lesions were visible in the lungs of 2 of 4 macaques (Fig. 3b, c). Additionally, all macaques had an increased ratio of lung weight to body weight (Fig. 3d) as compared to healthy rhesus macaques, indicative of pulmonary oedema. Histologically, 3 of the 4 macaques euthanized at 3 dpi developed some degree of pulmonary pathology. The lesions represented multifocal (Extended Data Fig. 4a), mild-to-moderate interstitial pneumonia that frequently centred on terminal bronchioles. The pneumonia was characterized by thickening of alveolar septa by oedema fluid and fibrin, and small-to-moderate numbers of macrophages and fewer neutrophils. Lungs with moderate changes also had alveolar oedema and fibrin with formation of hyaline membranes. There was minimal type-II pneumocyte hyperplasia. Occasionally, bronchioles showed necrosis, and the loss and attenuation of the epithelium with infiltrates of neutrophils, macrophages and eosinophils. Within the multifocal lesions, there were perivascular infiltrates of small numbers of lymphocytes that formed perivascular cuffs (Extended Data Fig. 4b), and minimal-to-mild, multifocal hyperplasia of bronchiolar-associated lymphoid tissue. Three of 4 macaques at 3 dpi had fibrous adhesions of the lung to the pleura. Histological evaluation showed these adhesions to be composed of mature collagen interspersed with small blood vessels; therefore, this is most probably a chronic change rather than being related to infection with SARS-CoV-2. We observed minimal-to-mild inflammation in the upper airways with multifocal squamous metaplasia of the respiratory epithelium and infiltration of small numbers of neutrophils (Extended Data Fig. 5).

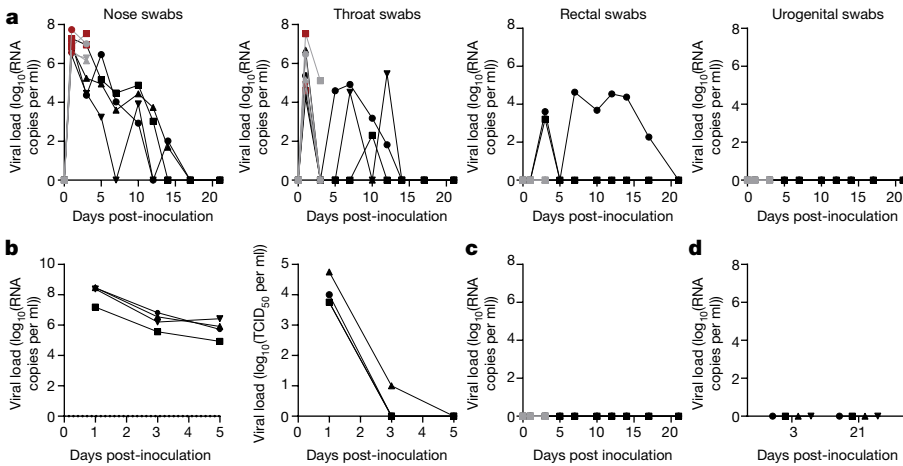


Fig. 2 | Viral loads in respiratory samples and bodily fluids. **a**, After inoculation, nose, throat, rectal and urogenital swabs were collected; viral loads in these samples were determined by quantitative reverse-transcription PCR. **b**, At 1, 3 and 5 dpi, bronchoalveolar lavages were performed on the 4 macaques that remained in the study through to 21 dpi; viral loads (left) and

virus titres (right) were determined in these samples. **c, d**, Viral loads were determined in blood collected during clinical examinations (**c**) and urine collected at necropsy at 3 and 21 dpi (**d**). Grey, macaques that were euthanized at 3 dpi ($n=4$); black, macaques that were euthanized at 21 dpi ($n=4$); red, virus was isolated from these samples.

Immunohistochemistry using a monoclonal antibody against SARS-CoV demonstrated viral antigen in small numbers of type-I and -II pneumocytes, as well as in alveolar macrophages. We detected antigen-positive macrophages in the mediastinal lymph nodes of three of four macaques (Fig. 3k). We also detected small numbers of antigen-positive lymphocytes and macrophages in the lamina propria of the intestinal tract of all four macaques. In one macaque, all the tissues of the gastrointestinal tract that we collected showed these antigen-positive mononuclear cells (Extended Data Fig. 6).

We performed ultrastructural analysis of lung tissue by transmission electron microscopy, which confirmed the histological diagnosis of interstitial pneumonia. The alveolar interstitial space was greatly expanded by oedema, fibrin, macrophages and neutrophils (Extended Data Fig. 7a). The subepithelial basement membrane was unaffected and maintained a consistent thickness and electron density. We occasionally observed type-I pneumocytes separated from the basement membrane by oedema; the resulting space sometimes contains virions. Affected type-I pneumocytes are lined by small-to-moderate numbers of virions that are 90–160 nm in diameter, with an electron-dense core bound by a less-dense capsid (Extended Data Fig. 7b–e). Alveolar spaces adjacent to affected pneumocytes are filled with a granular, moderately electron-dense material that is consistent with oedema fluid.

Replication in the respiratory tract

All tissues ($n=37$) collected at necropsy were analysed for the presence of viral RNA. At 3 dpi, high viral loads were detected in the lungs of all macaques (Extended Data Fig. 8a); virus was isolated from the lungs of all four macaques at this time. Additionally, viral RNA was detected in other samples from throughout the respiratory tract (Extended Data Fig. 8), as well as in lymphoid and gastrointestinal tissues. Viral RNA was not detected in other major organs, including the central nervous system. To distinguish viral RNA derived from respiratory secretions from active virus replication, we tested all samples with a presence of viral RNA for the presence of viral mRNA (Extended Data Fig. 8). We detected viral mRNA in all of the respiratory tissues but not in the gastrointestinal tissues (except for the stomach of one macaque), which indicates that virus replication in these tissues is unlikely—although we cannot exclude this possibility, owing to the limited sample size. By 21 dpi, viral RNA—but not mRNA—could still be detected in tissues from all four macaques (Extended Data Fig. 8g).

Serology

We analysed serum for the development of IgG against the SARS-CoV-2 spike protein in an enzyme-linked immunosorbent assay. By 10 dpi, all 4 macaques had seroconverted to the SARS-CoV-2 spike protein; neutralizing responses also started to appear at 10 dpi (Extended Data Fig. 9). The macaque with the lowest and latest neutralizing-antibody response was the one with prolonged viral shedding from the intestinal tract.

Discussion

Clinically, cases of COVID-19 range from being asymptomatic through to mild or severe manifestations^{5,6,8,9,13,16}. Patients present with influenza-like symptoms (such as fever and shortness of breath) and may develop pneumonia, requiring mechanical ventilation and support in an intensive care unit⁹. Similar to the diseases caused by infections with SARS-CoV and MERS-CoV, comorbidities such as hypertension and diabetes have an important role in adverse outcomes of COVID-19^{8,17,18}. In particular, advanced age and chronic conditions are indicators of a negative outcome^{5,7–9,16}—conditions that were absent in our healthy rhesus macaques. An analysis of 1,099 cases of COVID-19 from China has shown that approximately 5% of diagnosed patients developed severe pneumonia that required attending an intensive care unit, 2.3% required mechanical ventilation and 1.4% died⁹. The transient, moderate disease that we observed here in rhesus macaques is thus consistent with the majority of cases of COVID-19 in humans. Pulmonary infiltrates on radiographs—a hallmark of human infection with SARS-CoV-2^{4,6,7,9,10,16}—were observed in all macaques. The shedding pattern observed in rhesus macaques is notably similar to that previously observed in humans^{11,12}. In humans, consistent and high SARS-CoV-2 shedding has been observed from the upper and lower respiratory tract; frequent intermediate shedding has been observed from the intestinal tract; and there has been sporadic detection of SARS-CoV-2 in blood⁵. Similar to humans, the shedding of SARS-CoV-2 in macaques continued after resolution of clinical signs and radiological abnormalities¹⁹. Limited histopathology is available from patients with COVID-19^{20,21}. Our analysis of the histopathological changes observed in the lungs of rhesus macaques suggests that these changes resemble those observed in macaques infected with SARS-CoV and MERS-CoV^{21–24}, with regard to lesion type and cell tropism.

Serological responses in humans are not typically detectable before 6 days after the onset of symptoms; IgG titres of between

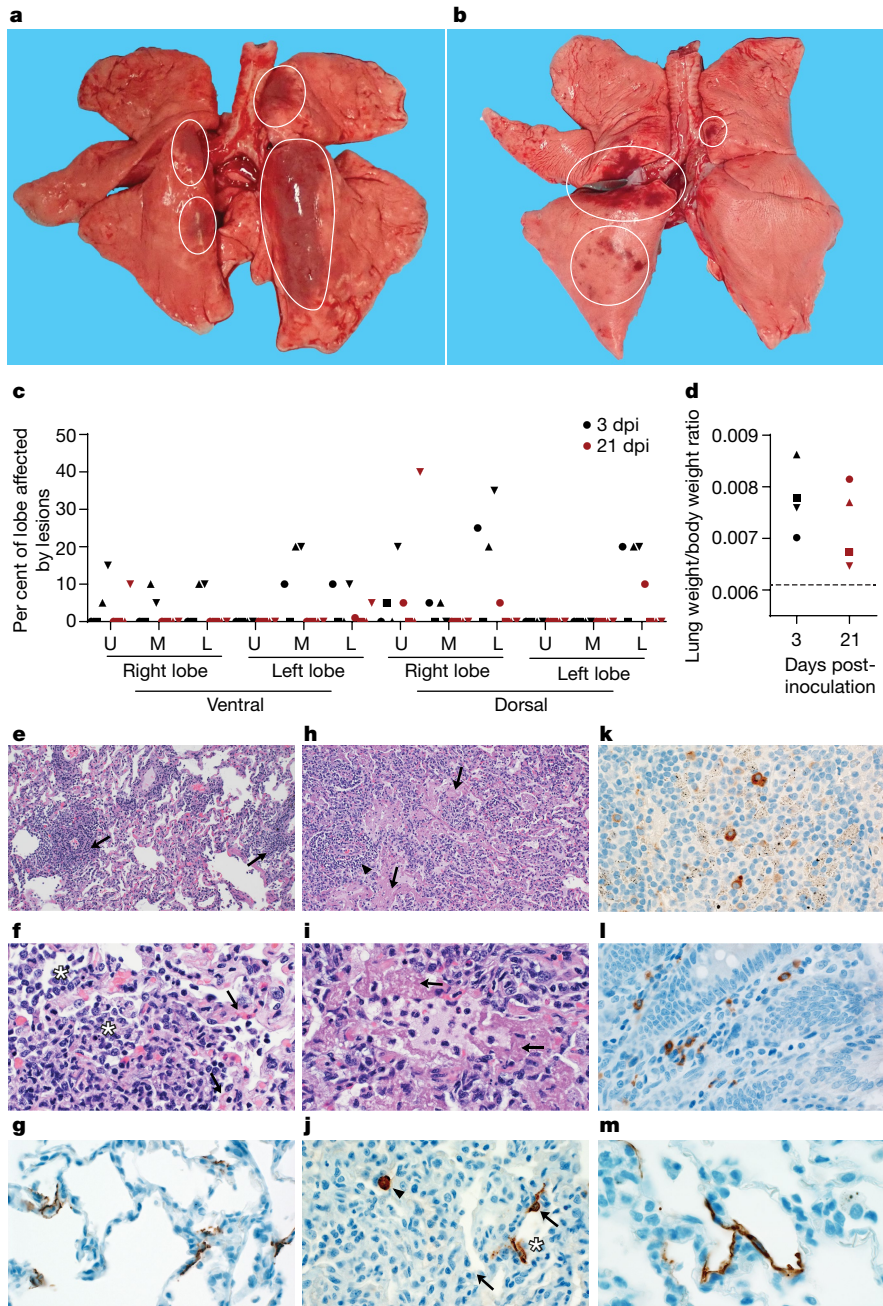


Fig. 3 | Pathological changes in rhesus macaques infected with SARS-CoV-2.

Four rhesus macaques were euthanized at 3 and 21 dpi. **a, b**, The lungs showed focal areas of hilar consolidation and hyperaemia (circles) at 3 dpi (**a**) and multifocal, random consolidation and hyperaemia (circles) at 21 dpi (**b**). The percentage of the area of the lungs affected by gross lesions was estimated (**c**), and the lung weight-to-bodyweight ratio was calculated (**d**). The dotted line represents the baseline ratio calculated from an in-house collection of lung and body weights from rhesus macaques with normal lungs. **e–i**, Histological analysis was performed on tissues collected at 3 dpi. Tissue sections were collected from the same anatomical location for each macaque; three tissue sections were prepared from each of the six lung lobes. In total, 18 lung sections were evaluated for each macaque; representative images are displayed. **e**, Pulmonary vessels surrounded by moderate numbers of lymphocytes, and fewer macrophages (arrows). **f**, Alveoli filled with

small-to-moderate numbers of macrophages and neutrophils (asterisks). The adjacent alveolar interstitium (arrows) is thickened by oedema, fibrin, neutrophils, lymphocytes and macrophages. **g**, SARS-CoV-2 antigen detected by immunohistochemistry in type-I pneumocytes. **h**, Pulmonary vessels bounded by lymphocytes (arrowhead) and hyaline membranes (arrows) line the alveolar spaces. **i**, Hyaline membranes line the alveoli (arrows). **j**, SARS-CoV-2 antigen detected by immunohistochemistry in type-I pneumocytes (asterisk) and type-II pneumocytes (arrow), as well as in alveolar macrophages (arrowheads). **k**, SARS-CoV-2 antigen detected by immunohistochemistry in macrophages in a mediastinal lymph node. **l**, SARS-CoV-2 antigen detected by immunohistochemistry in macrophages and lymphocytes in the lamina propria of the caecum. **m**, SARS-CoV-2 detected by immunohistochemistry in type-I pneumocytes. Magnification, 100 \times (**e, h**), 400 \times (**f, g, i–l**), 1,000 \times (**m**). U, upper; M, middle; L, lower.

100 and 10,000 have been observed after 12 to 21 days^{25,26}. Neutralizing titres were generally between 20 and 160. This corresponds to the results in our rhesus-macaque model, in which IgG responses were detected at around 7–10 dpi. Seroconversion was not directly followed by a decline in viral loads, as observed in patients with COVID-19^{5,26}.

Together, our rhesus-macaque model recapitulates COVID-19 in humans with regard to virus replication and shedding, the presence of pulmonary infiltrates, histological lesions and seroconversion. This extensive dataset enables us to bridge between the rhesus-macaque model and the disease observed in humans, and to use this model to assess the efficacy of medical countermeasures.

Online content

Any methods, additional references, Nature Research reporting summaries, source data, extended data, supplementary information, acknowledgements, peer review information; details of author contributions and competing interests; and statements of data and code availability are available at <https://doi.org/10.1038/s41586-020-2324-7>.

1. Wu, F. et al. A new coronavirus associated with human respiratory disease in China. *Nature* **579**, 265–269 (2020).
2. Zhu, N. et al. A novel coronavirus from patients with pneumonia in China, 2019. *N. Engl. J. Med.* **382**, 727–733 (2020).
3. WHO. *Coronavirus disease (COVID-19) situation reports*, <https://www.who.int/emergencies/diseases/novel-coronavirus-2019/situation-reports/> (2020).
4. Yang, W. et al. Clinical characteristics and imaging manifestations of the 2019 novel coronavirus disease (COVID-19): a multi-center study in Wenzhou city, Zhejiang, China. *J. Infect.* **80**, 388–393 (2020).
5. Yang, X. et al. Clinical course and outcomes of critically ill patients with SARS-CoV-2 pneumonia in Wuhan, China: a single-centered, retrospective, observational study. *Lancet Respir. Med.* **8**, 475–481 (2020).
6. Silverstein, W. K., Stroud, L., Cleghorn, G. E. & Leis, J. A. First imported case of 2019 novel coronavirus in Canada, presenting as mild pneumonia. *Lancet* **395**, 734 (2020).
7. Arentz, M. et al. Characteristics and outcomes of 21 critically ill patients with COVID-19 in Washington state. *J. Am. Med. Assoc.* (2020).
8. Zhou, F. et al. Clinical course and risk factors for mortality of adult inpatients with COVID-19 in Wuhan, China: a retrospective cohort study. *Lancet* **395**, 1054–1062 (2020).
9. Guan, W. J. et al. Clinical characteristics of coronavirus disease 2019 in China. *N. Engl. J. Med.* **382**, 1708–1720 (2020).
10. Shi, H. et al. Radiological findings from 81 patients with COVID-19 pneumonia in Wuhan, China: a descriptive study. *Lancet Infect. Dis.* **20**, 425–434 (2020).
11. Zou, L. et al. SARS-CoV-2 viral load in upper respiratory specimens of infected patients. *N. Engl. J. Med.* **382**, 1177–1179 (2020).
12. Kim, J. Y. et al. Viral load kinetics of SARS-CoV-2 infection in first two patients in Korea. *J. Korean Med. Sci.* **35**, e86 (2020).
13. Tang, A. et al. Detection of novel coronavirus by RT-PCR in stool specimen from asymptomatic child, China. *Emerg. Infect. Dis.* **26**, 1337–1339 (2020).
14. Harcourt, J. et al. Severe acute respiratory syndrome coronavirus 2 from patient with coronavirus disease, United States. *Emerg. Infect. Dis.* **26**, 1266–1273 (2020).
15. Everds, N. E. et al. Interpreting stress responses during routine toxicity studies: a review of the biology, impact, and assessment. *Toxicol. Pathol.* **41**, 560–614 (2013).
16. Wang, D. et al. Clinical characteristics of 138 hospitalized patients with 2019 novel coronavirus-infected pneumonia in Wuhan, China. *J. Am. Med. Assoc.* (2020).
17. Assiri, A. et al. Epidemiological, demographic, and clinical characteristics of 47 cases of Middle East respiratory syndrome coronavirus disease from Saudi Arabia: a descriptive study. *Lancet Infect. Dis.* **13**, 752–761 (2013).
18. Booth, C. M. et al. Clinical features and short-term outcomes of 144 patients with SARS in the greater Toronto area. *J. Am. Med. Assoc.* **289**, 2801–2809 (2003).
19. Lan, L. et al. Positive RT-PCR test results in patients recovered from COVID-19. *J. Am. Med. Assoc.* (2020).
20. Tian, S. et al. Pulmonary pathology of early-phase 2019 novel coronavirus (COVID-19) pneumonia in two patients with lung cancer. *J. Thorac. Oncol.* **15**, 700–704 (2020).
21. Xu, Z. et al. Pathological findings of COVID-19 associated with acute respiratory distress syndrome. *Lancet Respir. Med.* **8**, 420–422 (2020).
22. Ng, D. L. et al. Clinicopathologic, immunohistochemical, and ultrastructural findings of a fatal case of Middle East respiratory syndrome coronavirus infection in the United Arab Emirates, April 2014. *Am. J. Pathol.* **186**, 652–658 (2016).
23. Nicholls, J. M. et al. Lung pathology of fatal severe acute respiratory syndrome. *Lancet* **361**, 1773–1778 (2003).
24. Ding, Y. et al. The clinical pathology of severe acute respiratory syndrome (SARS): a report from China. *J. Pathol.* **200**, 282–289 (2003).
25. Wölfel, R. et al. Virological assessment of hospitalized cases of coronavirus disease 2019. *Nature* **581**, 465–469 (2020).
26. Zhao, Y. et al. Antibody responses to SARS-CoV-2 in patients of novel coronavirus disease 2019. *Clin. Infect. Dis.* <https://doi.org/10.1093/cid/ciaa344> (2020).

Publisher's note Springer Nature remains neutral with regard to jurisdictional claims in published maps and institutional affiliations.

© This is a U.S. government work and not under copyright protection in the U.S.; foreign copyright protection may apply 2020

Methods

Because this is an animal model with no prior data, statistical methods could not be used to predetermine sample size.

Ethics and biosafety statement

All experiments in macaques were approved by the Institutional Animal Care and Use Committee of Rocky Mountain Laboratories (National Institutes of Health (NIH)) and carried out by certified staff in an Association for Assessment and Accreditation of Laboratory Animal Care International-accredited facility, according to the institution's guidelines for animal use, following the guidelines and basic principles in the NIH Guide for the Care and Use of Laboratory Animals, the Animal Welfare Act, and the United States Department of Agriculture and the United States Public Health Service Policy on Humane Care and Use of Laboratory Animals. Rhesus macaques were housed in adjacent individual primate cages allowing social interactions, in a climate-controlled room with a fixed light/dark cycle (12-h light/12-h dark). Macaques were monitored at least twice daily throughout the experiment. Commercial monkey chow, treats and fruit were provided twice daily by trained personnel. Water was available ad libitum. Environmental enrichment consisted of a variety of human interaction, manipulanda, commercial toys, videos and music. The Institutional Biosafety Committee (IBC) approved work with infectious SARS-CoV-2 strains under biosafety level 3 conditions. Sample inactivation was performed according to IBC-approved standard operating procedures for removal of specimens from high containment.

Study design

To evaluate the use of rhesus macaques as a model for SARS-CoV-2, eight adult rhesus macaques (4 males, and 4 females, age 4–6 years) were inoculated via a combination of intranasal (0.5 ml per nostril), intratracheal (4 ml), oral (1 ml) and ocular (0.25 ml per eye) of a 4×10^5 50% tissue culture infectious dose (TCID₅₀) per ml (3×10^8 genome copies per ml) virus dilution in sterile DMEM. The macaques were observed twice daily for clinical signs of disease using a standardized scoring sheet (Supplementary Information, Supplementary Table 1); the same person assessed the macaques throughout the study. The predetermined endpoint for this experiment was 3 dpi for one group of 4 macaques, and 21 dpi for the remaining 4 macaques. Macaques were randomly assigned to a group for necropsy before the start of the experiment. Blinding was not used in this study as all macaques were subjected to the same treatment. Clinical examinations were performed on 0, 1, 3, 5, 7, 10, 12, 14, 17 and 21 dpi on anaesthetized macaques. On exam days, clinical parameters such as bodyweight, body temperature and respiration rate were collected, as well as ventrodorsal and lateral chest radiographs. Chest radiographs were interpreted by a board-certified clinical veterinarian. The following samples were collected at all clinical examinations: nasal, throat, urogenital and rectal swabs, and blood. The total white blood cell count, lymphocyte, neutrophil, platelet, reticulocyte and red blood cell counts, and haemoglobin and haematocrit values were determined from EDTA blood with the IDEXX ProCyte DX analyser (IDEXX Laboratories). Serum biochemistry (albumin, AST, ALT, GGT, BUN and creatinine) was analysed using the Piccolo Xpress Chemistry Analyzer and Piccolo General Chemistry 13 Panel discs (Abaxis). During clinical examinations on 1, 3, and 5 dpi, bronchoalveolar lavages were performed using 10 ml sterile saline. Bronchoalveolar lavages do not induce lung damage when spaced 48 h apart^{27,28}. After euthanasia, necropsies were performed. The percentage of gross lung lesions was scored by a board-certified veterinary pathologist and samples of the following tissues were collected: the inguinal lymph node, axillary lymph node, cervical lymph node, salivary gland, conjunctiva, nasal mucosa, oropharynx, tonsil, trachea, all six lung lobes, mediastinal lymph node, right and left bronchus, heart, liver, spleen, pancreas, adrenal gland, kidney, mesenteric lymph node,

stomach, duodenum, jejunum, ileum, caecum, colon, urinary bladder, reproductive tract (testes or ovaries depending on sex), bone marrow, frontal brain, cerebellum and brainstem. Histopathological analysis of tissue slides was performed by a board-certified veterinary pathologist blinded to the group assignment of the macaques.

Virus and cells

SARS-CoV-2 isolate nCoV-WA1-2020 (MN985325.1)¹⁴ (Vero passage 3) was provided by the Centers for Disease Control and Prevention, and propagated once in VeroE6 cells in DMEM (Sigma) supplemented with 2% fetal bovine serum (Gibco), 1 mM L-glutamine (Gibco), 50 U/ml penicillin and 50 µg/ml streptomycin (Gibco) (virus isolation medium). The virus stock used was 100% identical to the initial deposited GenBank sequence (MN985325.1) and no contaminants were detected. VeroE6 cells were maintained in DMEM supplemented with 10% fetal calf serum, 1 mM L-glutamine, 50 U/ml penicillin and 50 µg/ml streptomycin. VeroE6 cells were provided by R. Baric and were not authenticated in-house; mycoplasma testing is performed at regular intervals and no mycoplasma has been detected.

Quantitative PCR

RNA was extracted from swabs and bronchoalveolar lavage using the QiaAmp Viral RNA kit (Qiagen) according to the manufacturer's instructions. Tissues (30 mg) were homogenized in RLT buffer and RNA was extracted using the RNeasy kit (Qiagen) according to the manufacturer's instructions. For detection of viral RNA, 5 µl RNA was used in a one-step real-time RT-PCR E assay²⁹ using the Rotor-Gene probe kit (Qiagen) according to instructions of the manufacturer. In each run, standard dilutions of counted RNA standards were run in parallel, to calculate copy numbers in the samples. For detection of SARS-CoV-2 mRNA, primers targeting open reading frame 7 (ORF7) were designed as follows: forward primer 5'-TCCCAGGTAAACAAACCAACC-3', reverse primer 5'-GCTCACAAAGTAGCGAGTGTTAT-3', and probe FAM-ZEN-CTTGTAGATCTGTTCTCAAACGAAC-IBFQ. Five µl RNA was used in a one-step real-time RT-PCR using the Rotor-Gene probe kit (Qiagen) according to instructions of the manufacturer. In each run, standard dilutions of counted RNA standards were run in parallel, to calculate copy numbers in the samples.

Histopathology and immunohistochemistry

Histopathology and immunohistochemistry were performed on rhesus macaque tissues. After fixation for a minimum of 7 days in 10% neutral-buffered formalin and embedding in paraffin, tissue sections were stained with haematoxylin and eosin. To detect SARS-CoV-2 antigen, immunohistochemistry was performed using an anti-SARS nucleocapsid protein antibody (Novus Biologicals) at a 1:250 dilution. This antibody was first tested on SARS-CoV-2-infected and uninfected Vero E6 cell pellets, showing specific staining with infected cells and no staining with uninfected cells. The antibody showed specific staining with infected experimental tissue and no staining with uninfected tissue from rhesus macaques. Infected tissue and cell pellet specimens showed no staining when run with rabbit IgG controls (non-specific rabbit IgG substituted for primary antibody). Stained slides were analysed by a board-certified veterinary pathologist.

Transmission electron microscopy. After fixation for 7 days with Karnovsky's fixative at 4 °C, excised tissues were post-fixed for 1 h with 0.5% osmium tetroxide and 0.8% potassium ferricyanide in 0.1 M sodium cacodylate, washed 3 × 5 min with 0.1 M sodium cacodylate buffer, stained 1 h with 1% tannic acid, washed with buffer and then further stained with 2% osmium tetroxide in 0.1 M sodium cacodylate and overnight with 1% uranyl acetate at 4 °C. Specimens were dehydrated with a graded ethanol series with two final exchanges in 100% propylene oxide before infiltration and final embedding in Embed-812 and Araldite resin. Thin sections were cut with a Leica EM UC6 ultramicrotome (Leica),

Article

before viewing at 120 kV on a Tecnai BT Spirit transmission electron microscope (Thermo Fisher/FEI). Digital images were acquired with a Gatan Rio bottom mount digital camera system (Gatan) and processed using Adobe Photoshop v.CC 2019 (Adobe Systems).

Serum cytokine and chemokine analysis. Serum samples for analysis of cytokine and chemokine levels were inactivated with gamma radiation (2 MRad) according to standard operating procedures. Concentrations of granulocyte colony-stimulating factor, granulocyte-macrophage colony-stimulating factor, IFNy, IL-1 β , IL-1RA, IL-2, IL-4, IL-5, IL-6, IL-8, IL-10, IL-12/23 (p40), IL-13, IL-15, IL-17, MCP-1, MIP-1 α , MIP-1 β , soluble CD40-ligand (sCD40L), TGF α , TNF, VEGF and IL-18 were measured on a Bio-Plex 200 instrument (Bio-Rad) using the non-human primate cytokine MILLIPLEX map 23-plex kit (Millipore) according to the manufacturer's instructions.

Serology

Sera were analysed by SARS-CoV-2 spike (S) protein enzyme-linked immunosorbent assay (ELISA), as done previously for MERS-CoV³⁰. In brief, maxisorp (Nunc) plates were coated overnight with 100 ng/well S protein diluted in PBS³¹ (a gift of B. Graham) and blocked with blocker casein in PBS (Life Technologies). Sera were serially diluted in duplicate. SARS-CoV-2-specific antibodies were detected using anti-monkey IgG polyclonal antibody HRP-conjugated antibody (KPL), peroxidase-substrate reagent (KPL) and stop reagent (KPL). Optical density (OD) was measured at 405 nm. The threshold of positivity was calculated by taking the average of the day-0 values multiplied by 3.

For neutralization, sera were heat-inactivated (30 min, 56 °C) and twofold serial dilutions were prepared in 2% DMEM. Then, 100 TCID₅₀ of SARS-CoV-2 was added. After 60 min incubation at 37 °C, virus:serum mixture was added to VeroE6 cells and incubated at 37 °C and 5% CO₂. At 5 dpi, cytopathic effect was scored. The virus neutralization titre is expressed as the reciprocal value of the highest dilution of the serum that still inhibited virus replication. All sera were analysed in duplicate.

Reporting summary

Further information on research design is available in the Nature Research Reporting Summary linked to this paper.

Data availability

Data have been deposited in Figshare at <https://doi.org/10.35092/yhjc.12026910>.

27. Haley, P. J., Muggenborg, B. A., Rebar, A. H., Shopp, G. M. & Bice, D. E. Bronchoalveolar lavage cytology in cynomolgus monkeys and identification of cytologic alterations following sequential saline lavage. *Vet. Pathol.* **26**, 265–273 (1989).
28. Krombach, F. et al. Short-term and long-term effects of serial bronchoalveolar lavages in a nonhuman primate model. *Am. J. Respir. Crit. Care Med.* **150**, 153–158 (1994).
29. Corman, V. M. et al. Detection of 2019 novel coronavirus (2019-nCoV) by real-time RT-PCR. *Euro Surveill.* **25**, (2020).
30. van Doremalen, N. et al. High prevalence of Middle East respiratory coronavirus in young dromedary camels in Jordan. *Vector Borne Zoonotic Dis.* **17**, 155–159 (2017).
31. Wrapp, D. et al. Cryo-EM structure of the 2019-nCoV spike in the prefusion conformation. *Science* **367**, 1260–1263 (2020).

Acknowledgements We thank S. Gerber and N. Thornburg for providing the SARS-CoV-2 isolate used in this study; B. Graham, K. Corbett and O. Abiona for providing spike protein for serology; A. Mora for help with figure design, and staff of the Rocky Mountain Veterinary Branch (NIAID (NIH)) for animal care. This study was supported by the Intramural Research Program (NIAID (NIH)).

Author contributions V.J.M. and E.d.W. designed the study; V.J.M., F.F., B.N.W., N.v.D., L.P.P., J.S., K.M.-W., A.O., J.C., B.B., V.A.A., R.R., P.W.H., G.S., E.R.F., D.S. and E.d.W. acquired, analysed and interpreted the data; V.J.M., P.W.H., E.R.F., D.S. and E.d.W. wrote the manuscript. All authors have approved the submitted version.

Competing interests The authors declare no competing interests.

Additional information

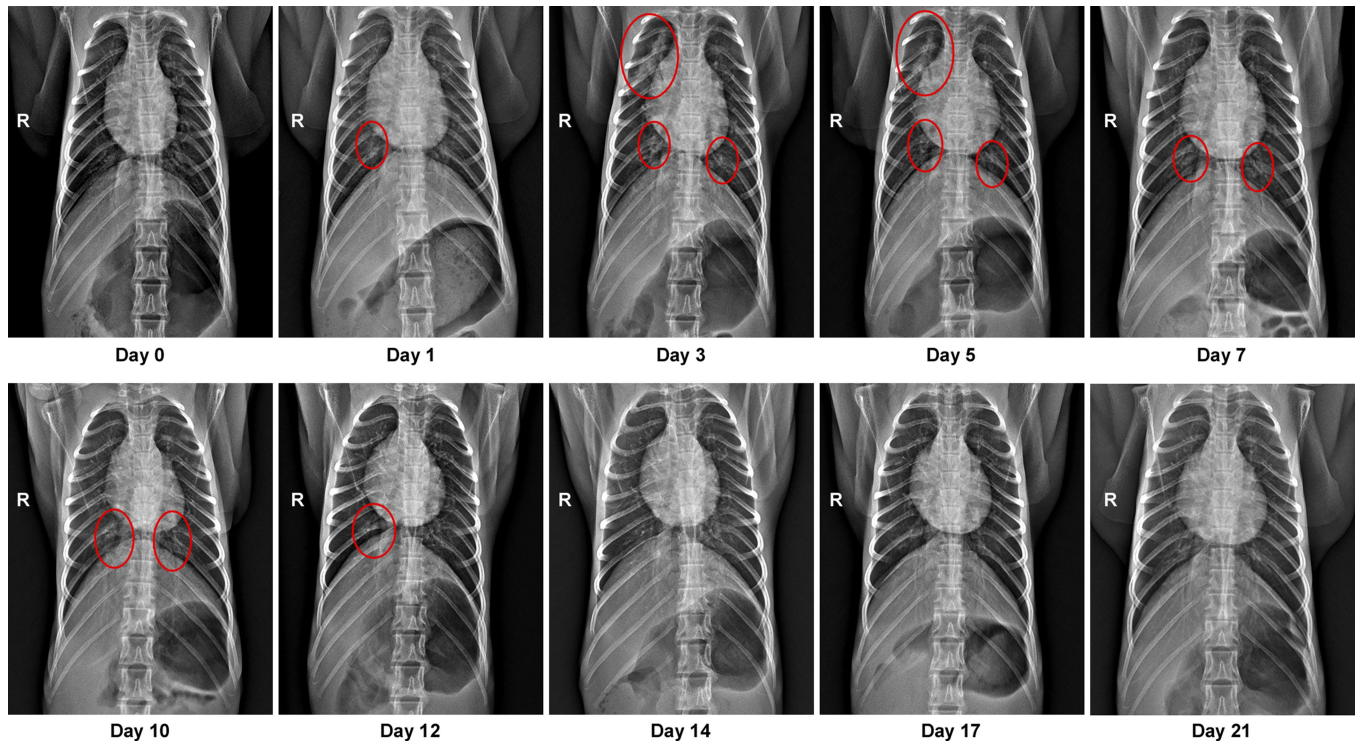
Extended data is available for this paper at <https://doi.org/10.1038/s41586-020-2324-7>.

Supplementary information is available for this paper at <https://doi.org/10.1038/s41586-020-2324-7>.

Correspondence and requests for materials should be addressed to E.d.W.

Peer review information *Nature* thanks Wolfgang Baumgärtner, Menno D. de Jong and Patricia Pesavento for their contribution to the peer review of this work.

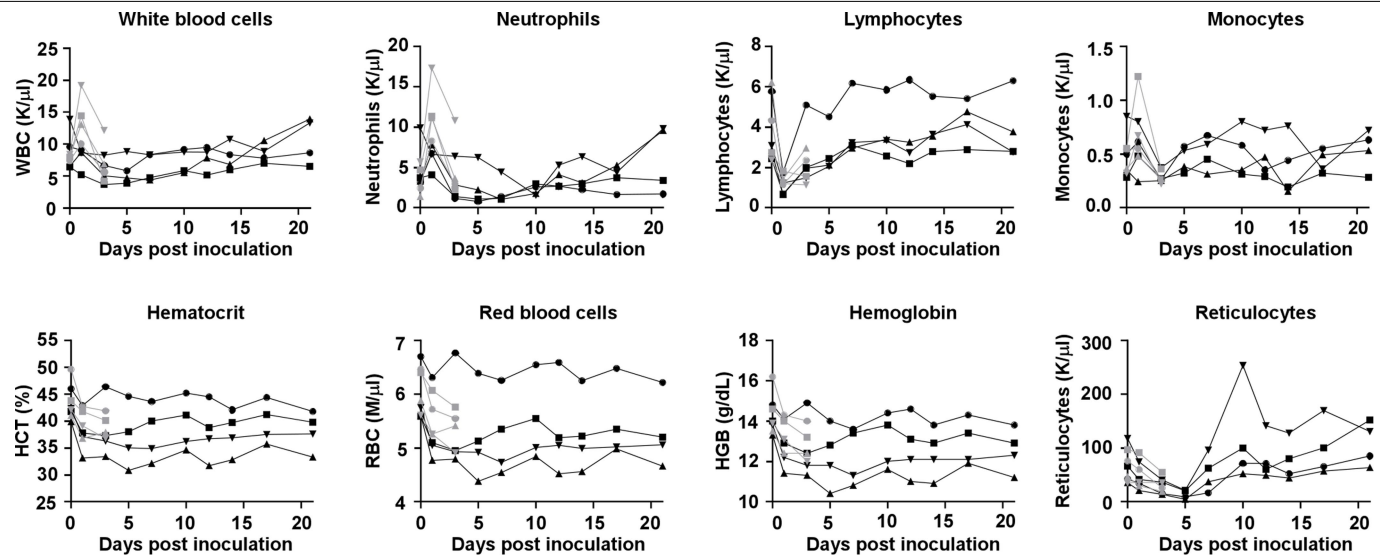
Reprints and permissions information is available at <http://www.nature.com/reprints>.



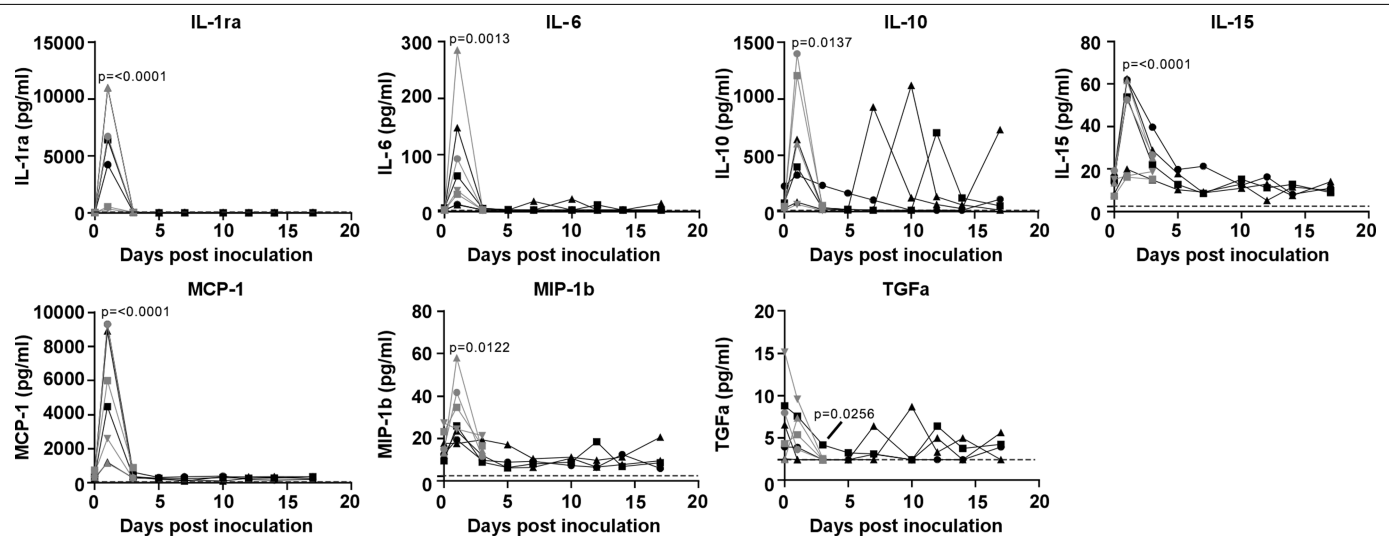
Extended Data Fig. 1 | Pulmonary infiltrates in a rhesus macaque after inoculation. Radiographs show the progression of pulmonary infiltrates throughout the study in a single macaque. This macaque is the one denoted by a black triangle throughout the Article. Circles indicate areas of

mild-to-moderate pulmonary infiltrates. R, right side of the macaque. Three chest radiographs were taken at each time point: right lateral, left lateral and ventrodorsal. Only the ventrodorsal radiograph is shown.

Article



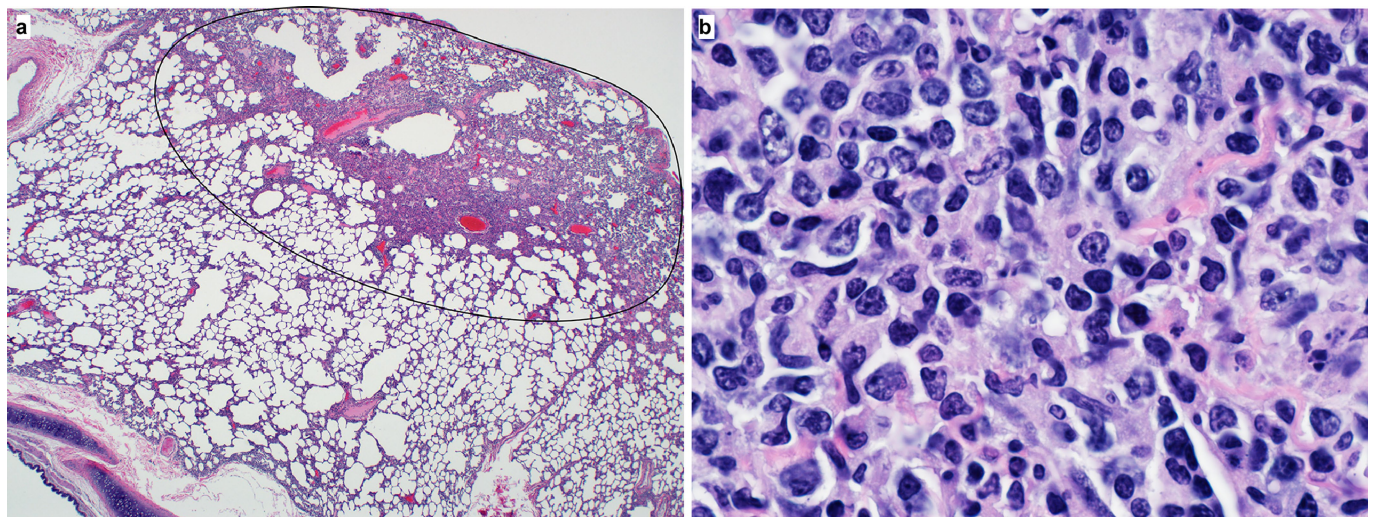
Extended Data Fig. 2 | Haematological changes in rhesus macaques infected with SARS-CoV-2. $n=8$ macaques at 0, 1 and 3 dpi, and $n=4$ macaques thereafter.



Extended Data Fig. 3 | Cytokine and chemokine levels in the serum of rhesus macaques infected with SARS-CoV-2. The levels of 23 cytokines and chemokines were determined in serum at different time points after inoculation. Levels are displayed only for those cytokines and chemokines for which statistically

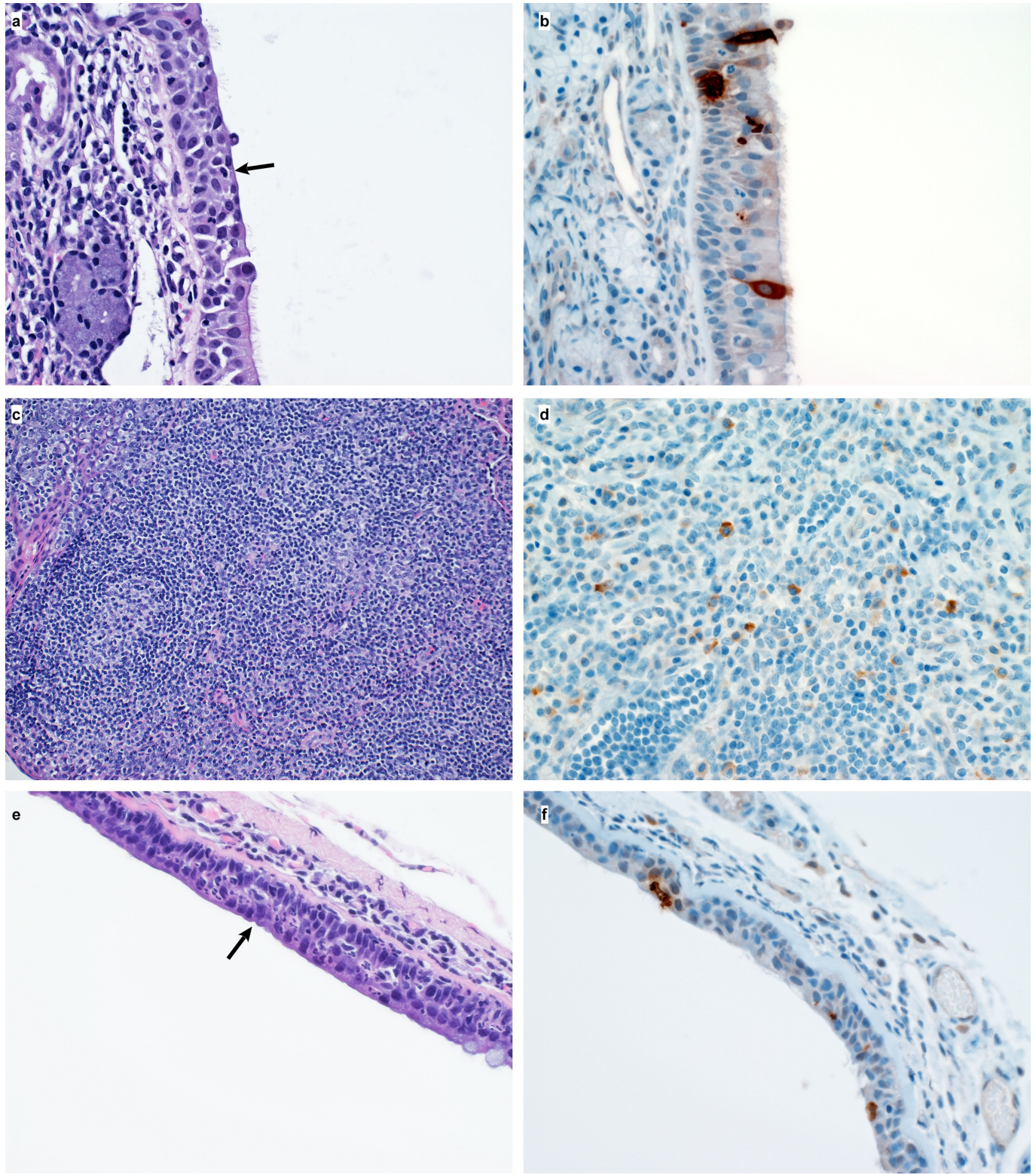
significant (one-way analysis of variance) differences were observed compared to levels on the day of inoculation. The lower limit of detection is indicated with a dotted line. Serum samples were analysed in duplicate from each macaque for each time point; $n = 8$ macaques at 0, 1, and 3 dpi and $n = 4$ macaques thereafter.

Article



Extended Data Fig. 4 | Histological lesions in the lungs of a rhesus macaque infected with SARS-CoV-2. **a**, This low-magnification figure displays the focal nature of SARS-CoV-2 lesions in the lungs of macaques euthanized at 3 dpi. The circle indicates the lung affected by lesion; the remaining lung tissue is healthy. **b**, Lymphocytes surround pulmonary vessels. Magnification, 500 \times . Tissue

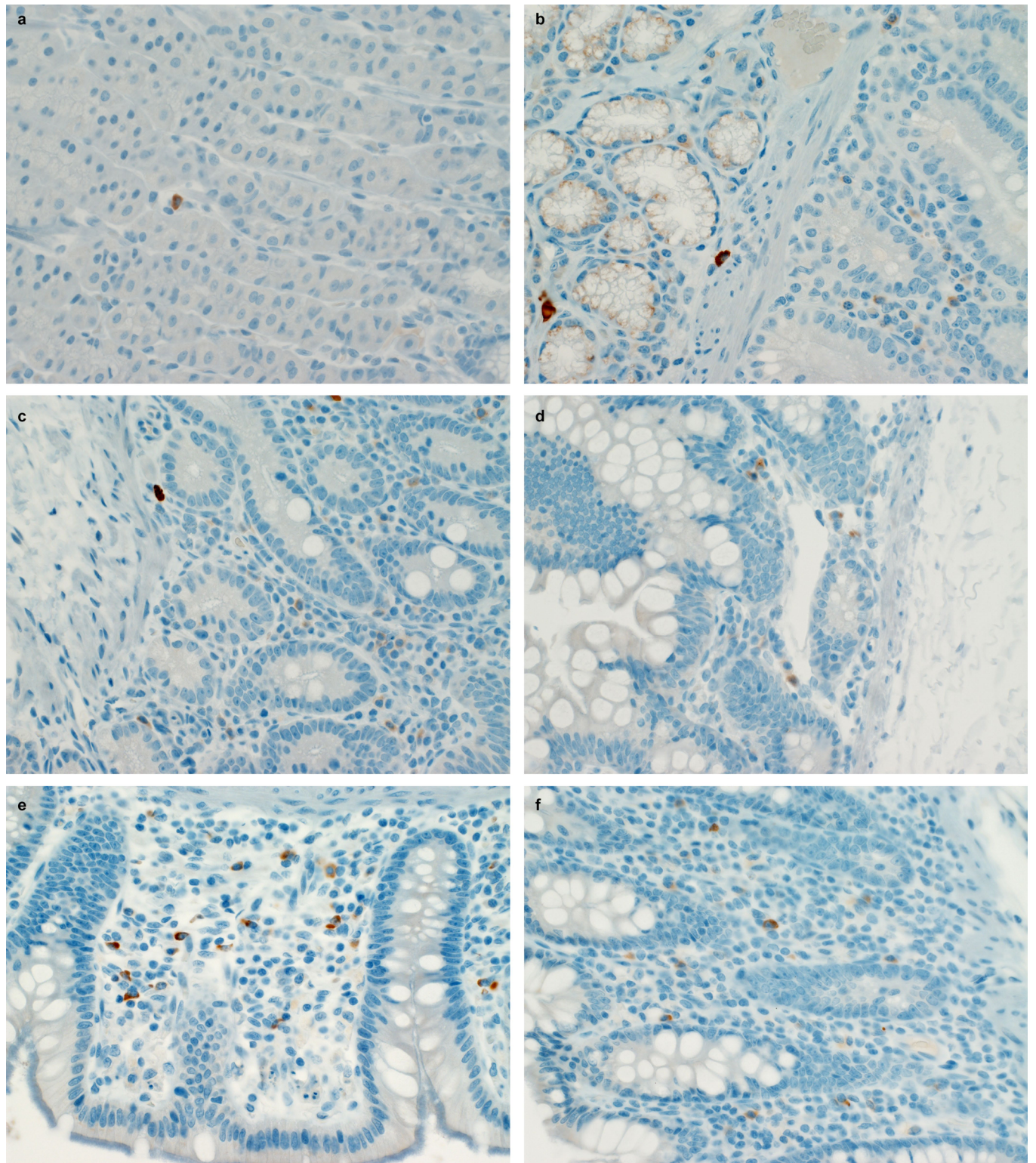
sections were collected from the same anatomical location for each macaque; three tissue sections were prepared from each of the six lung lobes. In total, 18 lung sections were evaluated for each macaque ($n=4$); representative images are displayed.



Extended Data Fig. 5 | Histological changes in the respiratory tract of rhesus macaques infected with SARS-CoV-2. **a**, Squamous metaplasia (arrow) of respiratory epithelium of the nasal turbinate. Magnification, 400×. **b**, SARS-CoV-2 antigen is detected by immunohistochemistry in respiratory epithelium of the nasal turbinate. Magnification, 400×. **c**, Essentially normal tonsil. Magnification, 400×. **d**, SARS-CoV-2 antigen is detected by immunohistochemistry in tonsillar macrophages. Magnification, 400×. **e**, Squamous metaplasia of tracheal

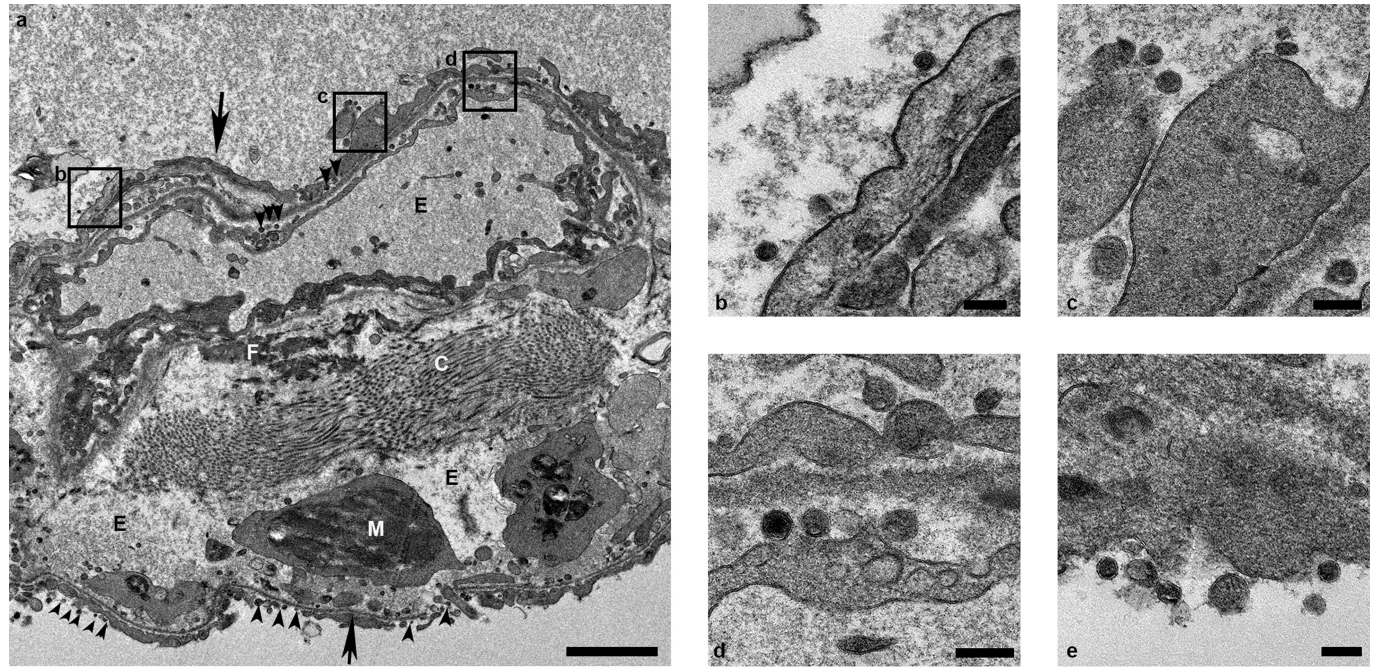
columnar epithelium (arrow). Magnification, 400×. **f**, SARS-CoV-2 antigen is detected by immunohistochemistry in tracheal columnar epithelium. Magnification, 400×. Tissue sections were collected from the same anatomical location for each macaque ($n=4$) and organ; one tissue section was evaluated of the nasal turbinates of each macaque; three tissue sections were evaluated from the tonsil and trachea.

Article



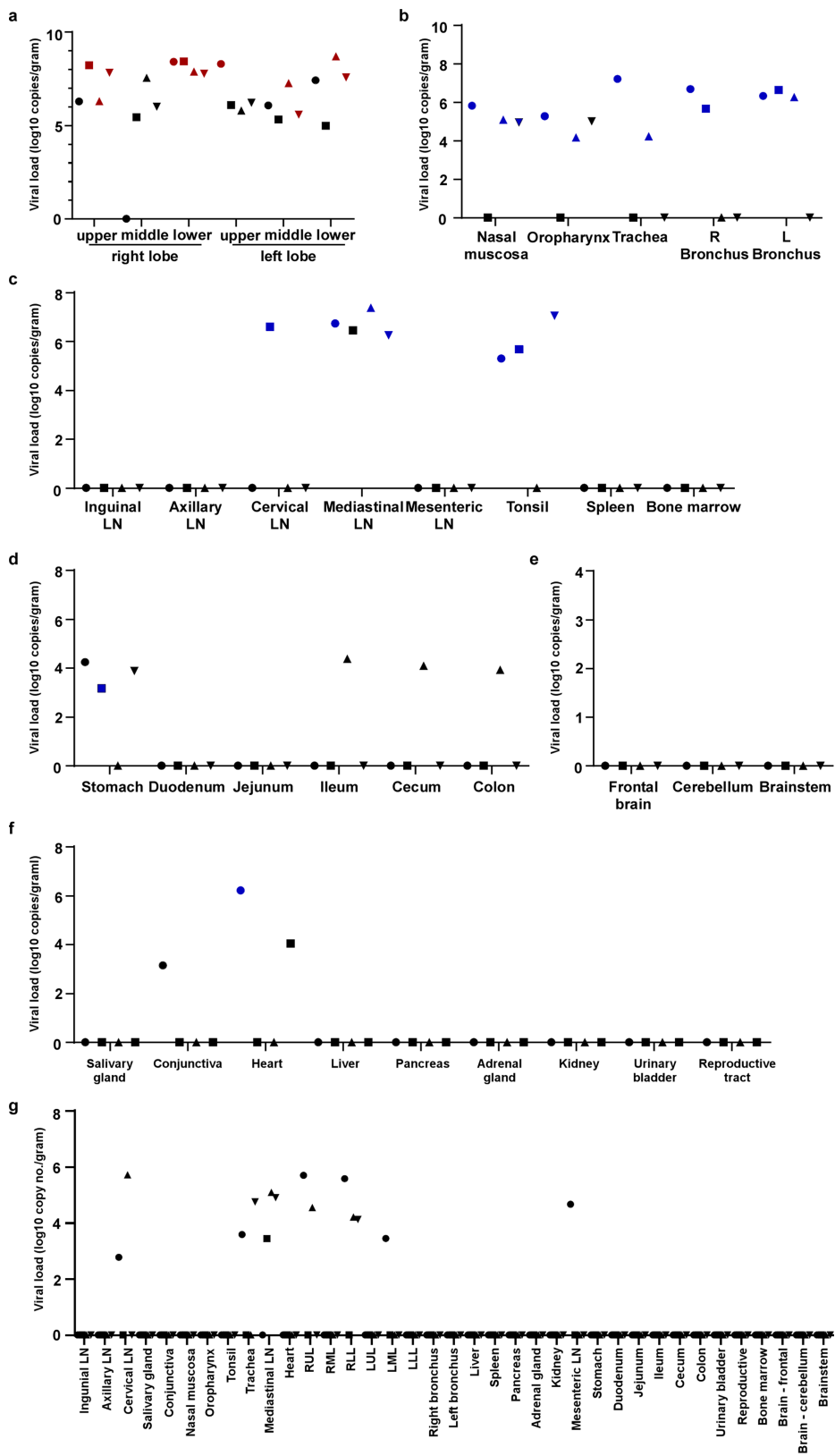
Extended Data Fig. 6 | SARS-CoV-2 antigen in the gastrointestinal tract of rhesus macaque infected with SARS-CoV-2. a–f, Mononuclear cells stained positive for SARS-CoV-2 antigen in the lamina propria of the stomach (a), duodenum (b), jejunum (c), ileum (d), caecum (e) and colon (f) of a macaque

infected with SARS-CoV-2 and euthanized on 3 dpi. Tissue sections were collected from the same anatomical location for each macaque ($n=4$) and organ; three tissue sections were evaluated from each macaque and organ.



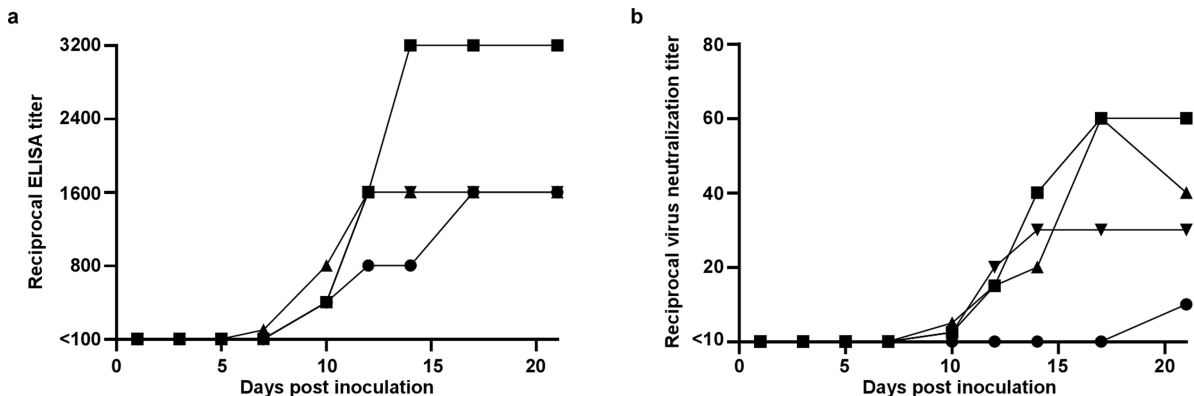
Extended Data Fig. 7 | Ultrastructural analysis of the lungs of rhesus macaques infected with SARS-CoV-2. **a–e,** Lung tissue collected on 3 dpi was analysed by transmission electron microscopy. The alveolar interstitium is expanded by oedema (E), fibrin (F) and mononuclear inflammatory cells (M) (**a**). Normal collagen fibres (**c**) and multiple virions (arrowheads) line type-I

pneumocytes (arrows). Boxes in **a** indicate areas enlarged in **b–d**. **b–e**, SARS-CoV-2 virions lining type-I pneumocytes. Scale bars, 2 μm (**a**), 0.2 μm (**b–e**). Three tissue samples were collected from each macaque ($n=4$) and cut into 6 samples for analysis; a minimum of 2 samples were analysed per macaque ($n=4$).



Extended Data Fig. 8 | Viral loads in tissues collected from rhesus macaques infected with SARS-CoV-2. Eight adult rhesus macaques were inoculated with the SARS-CoV-2 isolate nCoV-WA1-2020 and euthanized at 3 ($n=4$) or 21 ($n=4$) dpi. Thirty-seven tissues were collected at necropsy and analysed for the presence of viral RNA by quantitative reverse-transcription PCR (qRT-PCR). **a–g**, Tissues are grouped by lung lobes collected at 3 dpi (**a**) (red symbols indicate tissues from which virus could be isolated in Vero E6 cells); other tissues from the respiratory

tract at 3 dpi (**b**); lymphoid tissues at 3 dpi (**c**); gastrointestinal tissues at 3 dpi (**d**); the central nervous system at 3 dpi (**e**); the remaining tissues at 3 dpi (**f**); and all tissues collected at 21 dpi (**g**). Blue symbols in **b–g** indicate that viral mRNA was also detected in these tissues. L, left; LLL, left lower lung lobe; LML, left middle lung lobe; LN, lymph node; LUL, left upper lung lobe; R, right; RLL, right lower lung lobe; RML, right middle lung lobe; RUL, right upper lung lobe.



Extended Data Fig. 9 | Antibody response in rhesus macaques infected with SARS-CoV-2. **a, b,** Sera collected after inoculation were tested for the presence of IgG against SARS-CoV-2 spike in an ELISA (**a**) and for the presence of neutralizing antibodies in a microneutralization assay (**b**). All sera were analysed in duplicate.

Article

Extended Data Table 1 | Clinical signs observed in rhesus macaques inoculated with SARS-CoV-2

Animal	Clinical signs observed 1-6 dpi	Clinical signs observed 7-21 dpi	Observations at necropsy*
RM1	Hunched posture; piloerection; tachypnea; flushed appearance; red eyes; very agitated; reduced appetite; mildly dehydrated. Euthanized 3 dpi.	N/A	Gross lung lesions. Enlarged tonsils and mediastinal lymph nodes. Fluid-filled stomach, small and large intestine.
RM2	Piloerection; dyspnea; reduced appetite. Euthanized 3 dpi.	N/A	Fluid-filled stomach, small and large intestine.
RM3	Piloerection; tachypnea; flushed appearance; reduced appetite; mildly dehydrated. Euthanized 3 dpi.	N/A	Epistaxis. Gross lung lesions. Enlarged mediastinal lymph nodes. Fluid-filled stomach, small and large intestine.
RM4	Hunched posture; piloerection; tachypnea; dyspnea; reduced appetite. Euthanized 3 dpi.	N/A	Gross lung lesions. Foamy exudate from trachea. Enlarged mediastinal lymph nodes. Fluid-filled stomach, small and large intestine.
RM5	Hunched posture; piloerection; tachypnea; dyspnea; reduced appetite.	Tachypnea; dyspnea; reduced appetite; mildly dehydrated. Recovered on 9 dpi.	Gross lung lesions. Enlarged mesenteric lymph nodes.
RM6	Hunched posture; piloerection; tachypnea; dyspnea; reduced appetite; serous nasal discharge.	Piloerection; bradypnea; mildly dehydrated; crusty nasal discharge. Recovered on 10 dpi.	None.
RM7	Hunched posture; piloerection; pale appearance; tachypnea; dyspnea; irregular; labored respirations; anorexia; mildly dehydrated; serous nasal discharge.	Hunched posture; piloerection; pale appearance; tachypnea; dyspnea; reduced appetite; mildly dehydrated; crusty nasal discharge. Recovered on 17 dpi.	None.
RM8	Hunched posture; piloerection; pale appearance; increased, dyspnea; reduced appetite; serous nasal discharge.	Hunched posture; piloerection; pale appearance; increased, dyspnea; nasal discharge; reduced appetite; mildly dehydrated; serous nasal discharge. Recovered on 13 dpi.	Gross lung lesions.

*Incidental observations not related to infection with SARS-CoV-2 were omitted from this table.

Corresponding author(s): Emmie de Wit

Last updated by author(s): Mar 28, 2020

Reporting Summary

Nature Research wishes to improve the reproducibility of the work that we publish. This form provides structure for consistency and transparency in reporting. For further information on Nature Research policies, see [Authors & Referees](#) and the [Editorial Policy Checklist](#).

Statistics

For all statistical analyses, confirm that the following items are present in the figure legend, table legend, main text, or Methods section.

n/a Confirmed

- The exact sample size (n) for each experimental group/condition, given as a discrete number and unit of measurement
- A statement on whether measurements were taken from distinct samples or whether the same sample was measured repeatedly
- The statistical test(s) used AND whether they are one- or two-sided
Only common tests should be described solely by name; describe more complex techniques in the Methods section.
- A description of all covariates tested
- A description of any assumptions or corrections, such as tests of normality and adjustment for multiple comparisons
- A full description of the statistical parameters including central tendency (e.g. means) or other basic estimates (e.g. regression coefficient) AND variation (e.g. standard deviation) or associated estimates of uncertainty (e.g. confidence intervals)
- For null hypothesis testing, the test statistic (e.g. F , t , r) with confidence intervals, effect sizes, degrees of freedom and P value noted
Give P values as exact values whenever suitable.
- For Bayesian analysis, information on the choice of priors and Markov chain Monte Carlo settings
- For hierarchical and complex designs, identification of the appropriate level for tests and full reporting of outcomes
- Estimates of effect sizes (e.g. Cohen's d , Pearson's r), indicating how they were calculated

Our web collection on [statistics for biologists](#) contains articles on many of the points above.

Software and code

Policy information about [availability of computer code](#)

Data collection

No software was used.

Data analysis

Data were analyzed using Graphpad Prism 8.2.1

For manuscripts utilizing custom algorithms or software that are central to the research but not yet described in published literature, software must be made available to editors/reviewers. We strongly encourage code deposition in a community repository (e.g. GitHub). See the Nature Research [guidelines for submitting code & software](#) for further information.

Data

Policy information about [availability of data](#)

All manuscripts must include a [data availability statement](#). This statement should provide the following information, where applicable:

- Accession codes, unique identifiers, or web links for publicly available datasets
- A list of figures that have associated raw data
- A description of any restrictions on data availability

Data have been deposited in Figshare: <https://doi.org/10.35092/yhjc.12026910>

Field-specific reporting

Please select the one below that is the best fit for your research. If you are not sure, read the appropriate sections before making your selection.

Life sciences Behavioural & social sciences Ecological, evolutionary & environmental sciences

For a reference copy of the document with all sections, see nature.com/documents/nr-reporting-summary-flat.pdf

Life sciences study design

All studies must disclose on these points even when the disclosure is negative.

Sample size	Since this is a model with no prior data, it was not possible to perform a power analysis. The sample size was based on experience with other nonhuman primate models of respiratory disease.
Data exclusions	No data were excluded.
Replication	Lung histology: for each animal (n=4), 3 sections were evaluated from all 6 lung lobes. Gastrointestinal tract, trachea, tonsil histology: Tissue sections were collected from the same anatomical location for each animal (n=4) and organ; three tissue sections were evaluated from each animal and organ. Nasal turbinate histology: Tissue sections were collected from the same anatomical location for each animal (n=4) and organ; one tissue section was evaluated from each animal and organ. Radiographs: Three chest radiographs were taken from each animal at each clinical exam: right-lateral, left-lateral and ventro-dorsal; only the ventro-dorsal radiograph is shown. Cytokine analysis: serum samples were analyzed in duplicate from each animal for each timepoint; n= 8 animals on 0, 1, and 3 dpi and n=4 animals thereafter. Ultrastructural analysis: Three tissue samples were collected from each animal (n=4) and cut into 6 samples for analysis; a minimum of 2 samples were analyzed per animal (n=4). Serological analysis: Serum samples were analyzed in duplicate from each animal (n=4) for each timepoint.
Randomization	Animals were randomly assigned to the group euthanized at 3 dpi or 21 dpi.
Blinding	Blinding was not used since there was only a single treatment (inoculation with SARS-CoV-2).

Reporting for specific materials, systems and methods

We require information from authors about some types of materials, experimental systems and methods used in many studies. Here, indicate whether each material, system or method listed is relevant to your study. If you are not sure if a list item applies to your research, read the appropriate section before selecting a response.

Materials & experimental systems		Methods	
n/a	Involved in the study	n/a	Involved in the study
<input type="checkbox"/>	<input checked="" type="checkbox"/> Antibodies	<input type="checkbox"/>	<input checked="" type="checkbox"/> ChIP-seq
<input type="checkbox"/>	<input checked="" type="checkbox"/> Eukaryotic cell lines	<input type="checkbox"/>	<input checked="" type="checkbox"/> Flow cytometry
<input checked="" type="checkbox"/>	<input type="checkbox"/> Palaeontology	<input type="checkbox"/>	<input checked="" type="checkbox"/> MRI-based neuroimaging
<input type="checkbox"/>	<input checked="" type="checkbox"/> Animals and other organisms		
<input checked="" type="checkbox"/>	<input type="checkbox"/> Human research participants		
<input checked="" type="checkbox"/>	<input type="checkbox"/> Clinical data		

Antibodies

Antibodies used	anti-SARS nucleocapsid protein antibody; Novus Biologicals, cat.no. NB100-56576, lotno.111003003 anti-monkey IgG (gamma) antibody, peroxidase-labeled; KPL, cat.no. 5220-0333, lot no. 10329492
Validation	Validation of cross-reactivity of SARS-CoV to SARS-CoV-2 in IHC was done in-house by embedding SARS-CoV-2 infected Vero cells in histogel and producing and staining histology slides.

Eukaryotic cell lines

Policy information about cell lines	
Cell line source(s)	VeroE6: Ralph Baric, University of North Carolina, Chapel Hill, USA
Authentication	Not authenticated in-house.
Mycoplasma contamination	Mycoplasma testing confirmed negative at regular intervals.
Commonly misidentified lines (See ICLAC register)	No commonly misidentified cell lines were used.

Animals and other organisms

Policy information about [studies involving animals](#); [ARRIVE guidelines](#) recommended for reporting animal research

Laboratory animals	Rhesus macaques, Chinese origin, adult (4-6 years), 4 males, 4 females
Wild animals	No wild animals were used.
Field-collected samples	No samples were collected in the field.
Ethics oversight	All animal experiments were approved by the Institutional Animal Care and Use Committee of Rocky Mountain Laboratories, NIH and carried out by certified staff in an Association for Assessment and Accreditation of Laboratory Animal Care (AAALAC) International accredited facility, according to the institution's guidelines for animal use, following the guidelines and basic principles in the NIH Guide for the Care and Use of Laboratory Animals, the Animal Welfare Act, United States Department of Agriculture and the United States Public Health Service Policy on Humane Care and Use of Laboratory Animals.

Note that full information on the approval of the study protocol must also be provided in the manuscript.